THE JOURNAL OF PHYSICAL CHEMISTRY B

Article

pubs.acs.org/JPCB

Photoactivation of Cryptochromes from *Drosophila melanogaster* and *Sylvia borin*: Insight into the Chemical Compass Mechanism by Computational Investigation

Gongyi Hong[†,‡] and Ruth Pachter*[,†]

[†]Air Force Research Laboratory, Wright-Patterson Air Force Base, AFRL/RX, 3005 Hobson Way, Dayton, Ohio 45433, United States

[‡]General Dynamics Information Technology, Inc., 5100 Springfield Pike, Dayton, Ohio 45433, United States

Supporting Information

ABSTRACT: Although behavioral studies demonstrated light-induced magnetoreception in the insect *Drosophila melanogaster*, gaining insight into the possibility that a radical-pair mechanism accounts for the magnetic response of the cryptochrome (DmCry1) is complicated by a number of factors. In addition, the mechanism of magnetoreception for the cryptochrome from the garden warbler bird *Sylvia borin* (gwCry1a), which demonstrated a long-lived radical pair by transient optical absorption measurements, has also not been rationalized. To assess potential feasibility of a radical-pair mechanism in DmCry1 and gwCry1a, formed by excitation and electron transfer between a Trp-triad and flavin adenine dinucleotide (FAD), further separated by electron transfer within the triad, we applied a combination of theoretical methods, including homology modeling and molecular dynamics (MD) for structure refinement, high-level ab initio theory, and MD simulations using a polarizable force-field for prediction of pK_a and the electron transfer rate. Calculated excitation energies, followed by electron transfer in model compounds of DmCry1 that assume proton transfer in conjunction with electron transfer from Trp (W420) to FAD and the predicted pK_a for the proximate residue to FAD (Cys416), support a radical-pair mechanism. Furthermore, free-energy and reorganization energies for the Trp-triad in DmCry1 demonstrate facile electron transfer, explained by the local protein environment and exposure to solvent, which in turn enables a large enough distance separation for the radical-pair partners. Results for gwCry1a demonstrated the importance of accounting for relaxed excited-state geometries in validating the first stage of a radical-pair mechanism. This work provides insight into the so-called chemical compass mechanism to explain magnetic-field sensing in DmCry1 and gwCry1a, expanding on previous work on the cyrptochrome from the plant *Arabidopsis thaliana* (Solov'yov et al. *J. Am. Chem. Soc.* **2012**, *134*, 18046−18052. Solov'yov et al., *Sci. Rep.* **2014**, *4*, 1−8.).

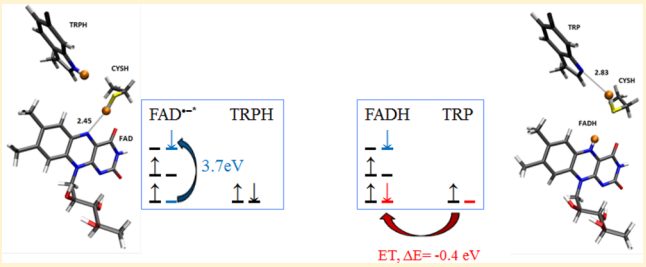

I. INTRODUCTION

The possibility that macroscopic cognitive species could respond to the weak geomagnetic field (ca. 50 μT) by quantum effects has drawn significant interest;[1,2] for example, *Erithacus rebecula* has a magnetic sense that acts as an inclination compass that is not sensitive to the field polarity.[3] Mechanistically, a chemical spin-correlated radical-pair compass formed in cryptochrome flavoprotein photoreceptors[4] upon photoactivation was suggested as the basis for magnetoreception[5] (see references therein). Radical-pairs are formed in cryptochromes between a flavin adenine dinucleotide (FAD) chromophore cofactor and proximate Trp within a conserved so-called Trp-triad by electron transfer from the triad, following electronic excitation of the FAD and subsequent protonation and deprotonation.[6] The resulting spin-correlated state is interconverted by hyperfine interactions with surrounding nuclei and can be modulated by a weak Zeeman interaction[7] that describes the alignment of the electron spins to the magnetic field; the spin Hamiltonian is given by $H = H_{\mathrm{Zeeman}} + H_{\mathrm{hyperfine}} + H_{\mathrm{dipolar}} + H_{\mathrm{exchange}} + H_{\mathrm{nuclear}}$ and $H_{\mathrm{Zeeman}} = \Sigma_{m=1}^{2}\mu_B g_m \boldsymbol{B}\cdot\boldsymbol{S}_m$ (μ_B, Bohr magneton; g_m, effective g factor of electron m (ca. 2); $\boldsymbol{S}_m$, electronic spin operators); $H_{\mathrm{hyperfine}} = \Sigma_{m=1}^{2}\Sigma_{k=1}^{N_m}\mu_B g_m \boldsymbol{S}_m\cdot\boldsymbol{A}_{m,k}\cdot\boldsymbol{I}_{m,k}$ ($\boldsymbol{A}_{m,k}$ hyperfine coupling tensor, $\boldsymbol{I}_{m,k}$ nuclear spin). Dipolar and exchange interactions are weak in this case as the radical-pair partners are separated by a large enough distance,[8] rationalized for the cryptochrome from *Arabidopsis thaliana* (AtCry1).[9] Time-resolved EPR spectroscopy has been useful in probing intermediates of the suggested mechanism.[10]

As noted in behavioral studies,[11] evidence is growing that avian magnetic sensing is consistent with a radical-pair mechanism. The response to weak oscillating magnetic fields superimposed on the static magnetic field can disrupt the response, providing further evidence.[12] A carotenoid−porphyrin−fullerene model system demonstrated that the lifetime of a photochemically formed radical-pair can indeed be altered by

Received: September 2, 2014
Revised: February 4, 2015
Published: February 24, 2015

DOI: 10.1021/jp508871h
J. Phys. Chem. B 2015, 119, 3883−3892

external weak magnetic fields.[13] Consistency with a radical-pair mechanism for AtCry1 was also demonstrated.[14,15] It was further shown[16] that with a suitable number of receptors to compensate for the signal attenuation through increased disorder, the systems are relatively robust, although there are still many open questions to be addressed.[2] Thus, there has been interest in understanding the mechanism's feasibility for various species, which could be potentially useful also for devising spin-based computation, data-storage or weak magnetic field sensing concepts through biomimetic systems.[17,18]

Interestingly, behavioral studies have shown that the cryptochrome is essential for its light-dependent magnetoreception in *Drosophila melanogaster* (DmCry1),[19] while transient optical absorption measurements showed that a long-lived radical-pair is formed in the cryptochrome from the garden warbler *Sylvia borin* (gwCry1a).[20] The active site of FAD and Trp-triad is conserved among cryptochromes from various species, as based on, for example, alignment[21] and superposition[22] of the X-ray crystal structures of AtCry1,[23] DmCry1,[24,25] and the mouse cryptochromes mCry2[26] and mCry1[27] (summarized in Table 1). In this context, we note that the edge-to-edge distances in the active site of DmCry1 are favorable for electron transfer (Figure 1S in the Supporting Infomation (SI)).[28]

Table 1. Root-Mean-Square Deviation (rmsd) Values Based on Superposition of the FAD Moiety, Proximate Residue, and Trp-Triad for Cryptochromes from AtCry1, mCry1, mCry1, and mCry2 using TM-Align[21] Following Sequence Alignment of This Region with BLAST[22a,b]

	W_f	W_m	W_n	proximate residue	rmsd
AtCry1	W324	W377	W400	D396	0.0
DmCry1	W342	W397	W420	C416	0.56
mCry1	W320	W374	W397	N393	0.68
mCry2	W338	W392	W415	N411	0.52

[a]Details of the X-ray structures used are summarized in section II.2. [b]Moieties in the active site for the radical-pair mechanism are described in **1A** in Figure 1 for DmCry1. W_n denotes the Trp nearest to FAD, W_f is the distant Trp, and W_m the middle Trp residue within the Trp-triad proximate to FAD.

However, although the radical-pair mechanism was investigated theoretically for a model compound of AtCry1 by Solov'yov et al.,[8,29] extrapolation of the understanding to other cryptochromes is complicated by notable differences. The cryptochrome in DmCry1 has a Cys proximate residue near the FAD's isoalloxazine moiety in the active site (described in Figure 1, **1A**) instead of Asp in AtCry1, while in gwCry1a, it comprises the Asn residue. The Cys residue for instance may mitigate the proton transfer supposition in AtCry1,[29] requiring careful assessment of the pK_a that takes into account the protein environment. Importantly, it was also proposed that for DmCry1 a radical anionic semiquinone ($FAD^{\bullet-}$) is excited,[30] also according to the absorption wavelength in the behavioral study,[31] unlike the oxidized forms in AtCry1[8,29] and gwCry1a.[20] In addition, an X-ray crystal structure for gwCry1a has not been reported.

In this work, we report for the first time an analysis of the radical-pair mechanism in cryptochromes from the insect *Drosophila melanogaster* and the bird *Sylvia borin*. Excitation energies and the electron transfer characteristics for model compounds that included the FAD moiety and part of the active site in DmCry1 were investigated, combined with pK_a calculations for the proximate residue to the isoalloxazine moiety, which provided support to the possibility of a radical-pair mechanism. Electron transfer within the Trp-triad following the initial electron transfer to FAD from the nearby Trp was examined by molecular dynamics (MD) free-energy simulations, indicating that the predicted electron transfer rates were fast and consistent with experimental results for homologous cryptochromes. The important role played by the local protein and aqueous environment was indicated in this case. Finally, results for the initial stage of a radical-pair mechanism in gwCry1a were rationalized, yet subject to taking into account relaxed excited-state geometries.

II. METHODS

II.1. Ab Initio Calculations. Electronic excitation in FAD was investigated using model compound **1B** and electron transfer from its nearby Trp residue (W_n) using model compounds **2A**, **2B**, and **2C** for DmCry1, gwCry1a, and AtCry1, respectively, as shown in Figure 1. Geometries in this case were derived from X-ray crystal structures or homology modeling, refined by MD simulations, and followed by density functional theory (DFT) geometry optimization, as described in Section II.2

Excitation energies of the model compounds, also upon electron transfer, were calculated by the equally weighted state-averaged over same spin-multiplicity complete active space SCF (CASSCF)[32] and extended multiconfiguration quasi-degenerate perturbation theory (XMCQDPT2)[33] based on the MCQDPT approach,[34] as implemented in Firefly,[35] partially based on GAMESS.[36] The active space was chosen using the principal-orbital complete active space protocol.[37] For neutral systems, namely, **1B** of FAD_{ox} and **2B** and **2C**, the active space included the HOMO of Trp and HOMO and LUMO for **1B** of FAD_{ox}. The three states were included in both CASSCF and XMCQDPT2 calculations. To explore all probable low excited states and to include static correlation as much as possible, for compounds containing semireduced flavin species such as **1B** of $FAD^{\bullet-}$ and **2A**, SOMO, SOMO-1, SOMO-2, LUMO, and LUMO+1 from **1B** of $FAD^{\bullet-}$ and HOMO of Trp were included in the active space, which resulted in a total of 75 doublet states for model compound **1B** of $FAD^{\bullet-}$ and 210 doublet states for **2A**; note that because at most 100 states were allowed, 100 doublet states for **2A** were adopted in state-averaged CASSCF calculations. Although a large number of states were included in the CASSCF calculations, only a few relevant low excited states were included in the expensive XMCQDPT2 calculations. The default EDSHFT value of 0.0 was used. MacMolPlt version 7.4.4[38] was used to characterize MOs.

II.2. Model Systems and MD Refinement. The **1B** FAD model compound (Figure 1) in the oxidized state was optimized using DFT with hybrid B3LYP, PBE0, and range-separated CAMB3LYP exchange-correlation functionals and Hartree−Fock (HF) with a 6-31G* basis set using Gaussian09.[39] To ensure accuracy of the geometry of **1B**, we calculated excitation energies of the oxidized state of **1B** using time-dependent DFT (TDDFT)[40] and CASSCF/XMCQDPT2 (described in Section II.1), as is summarized in Table 2. The relative order in the TDDFT excitation energies calculated with hybrid and range-separated functionals (6-31G* basis set) was as expected.[41] The excitation energy calculated by CASSCF-

DOI: 10.1021/jp508871h
J. Phys. Chem. B 2015, 119, 3883−3892

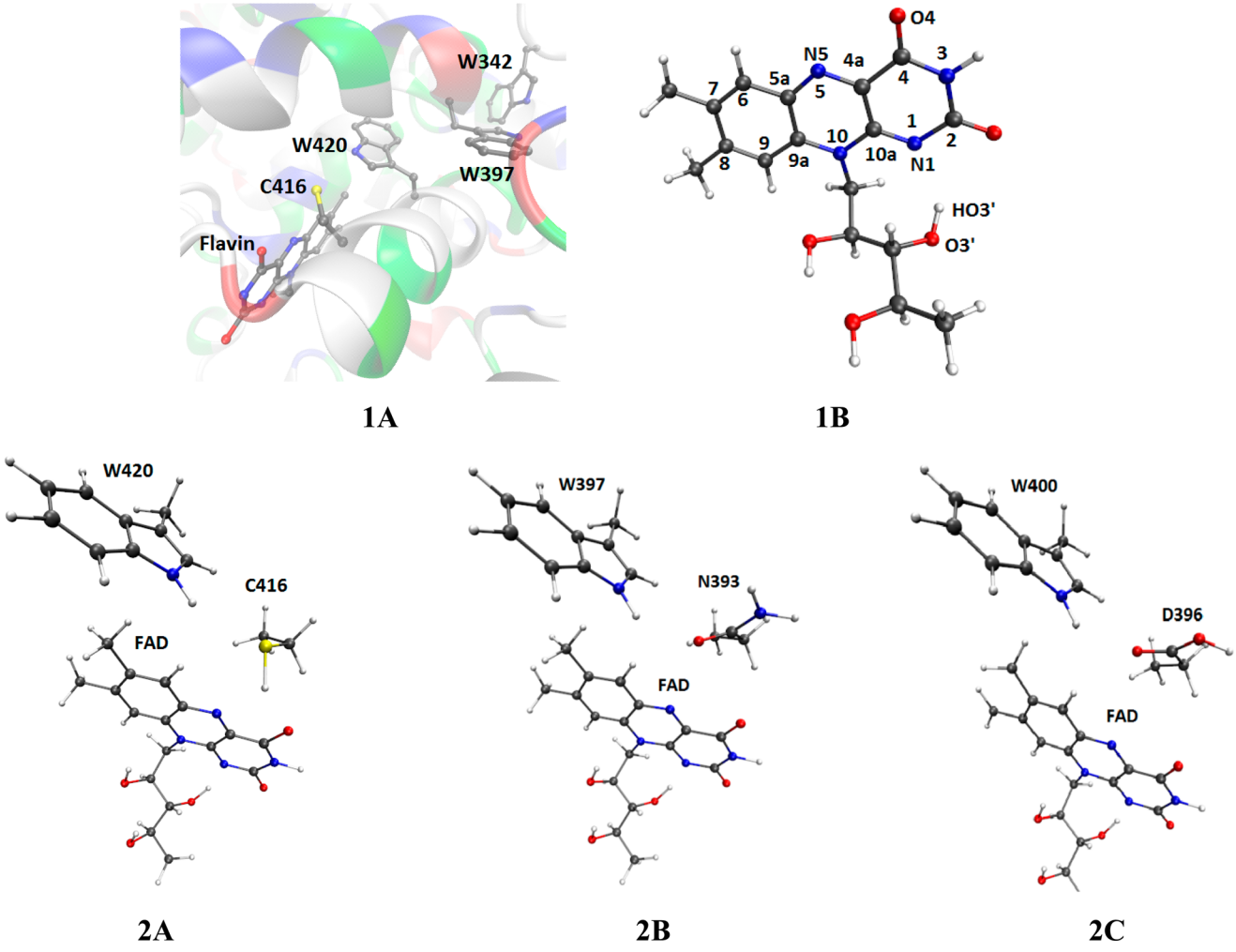

Figure 1. Active site of DmCry1 (**1A**) (see Table 1 for listing of proximate residue and W_n, W_m, and W_f residues) and model compound **1B**; model compounds **2A** (DmCry1), **2B** (gwCry1a), and **2C** (AtCry1); gray: C, blue: N, red: O, and white: H.

Table 2. $S_0 \rightarrow S_1$ Excitation Energies (eV) of Oxidized FAD Using Model Compound 1B Optimized Using DFT/B3LYP, PBE0, and CAMB3LYP Functionals and HF Level

	excitation energy			
geometry	TDDFT/B3LYP	TDDFT/PBE0	TDDFT/CAMB3LYP	CASSCF/XMCQDPT2[b]
B3LYP	3.05	3.15	3.42	3.22
PBE0	3.07	3.18	3.45	3.25
CAMB3LYP	3.10	3.21	3.50	3.34
HF	3.22(3.13)[a]	3.33(3.23)[a]	3.63(3.52)[a]	3.11

[a]Solvated in water with PCM. [b]Two electrons, two orbitals, and three states were used in the CASSCF/XMCQDPT2 calculations.

XMCQDPT2/6-31G* using the B3LYP geometry is in agreement with the experimentally determined excitation energy for oxidized FAD of ca. 2.8 eV in a phosphate buffer,[42] and this functional was therefore used for optimization of larger model compounds. The radical-anion state of the model compound was optimized at the UB3LYP/6-31+G* level with a doublet spin state.

For investigation of electron transfer from W420 to excited $FAD^{\bullet -}$* to form a radical-pair, a larger model compound was considered (**2A** in Figure 1), as feasible computationally, based on MD refinement of the DmCry1 crystal structure (pdb: 4GUA),[24,25] followed by DFT optimization. Molecular models were generated using VMD (visual molecular dynamics).[43] The RESP[44] charge of the semireduced state $FAD^{\bullet -}$ was used and the protein was solvated in a 9.64 × 9.15 × 8.16 nm^3 box. MD simulations were performed using GROMACS v4.5.4[45] with the force-fields Amber99SB[46] for the protein and GAFF[47] for FAD. Particle-mesh Ewald sums were applied for efficient treatment of long-range electrostatics with a short-range cutoff of 1 nm and a relative strength of the electrostatic interaction at the cutoff of 10^{-5} at 1 nm (spacing of 0.12 nm, interpolation order of 6). A 1.2 nm cutoff was used in calculating the Lennard-Jones potential. The LINCS algorithm was chosen to reset bonds to their correct lengths after an unconstrained update.[48] After energy optimization, the system was equilibrated for 10 ns at constant NVT (T = 300 K), where a velocity rescaling with a stochastic term of 0.1 ps was used to regulate the temperature.

DOI: 10.1021/jp508871h
J. Phys. Chem. B 2015, 119, 3883−3892

Model compounds were derived from the last snapshot of the MD trajectory, and subsequent geometry optimization was performed at the DFT level using UB3LYP/6-31+G* with constrained boundary carbon atoms. Model compounds of DmCry1 before (**2Aa**) and after (**2Ab**) proton transfer from Trp420 to FAD via Cys416, were considered (Figure 2). A

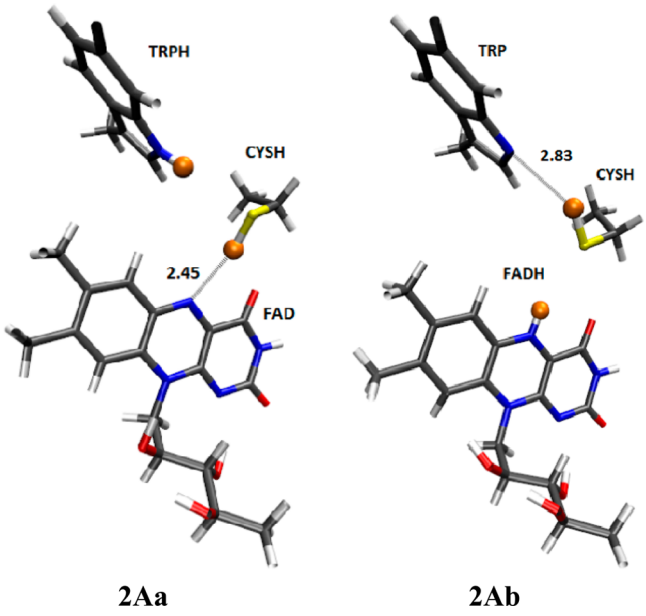

Figure 2. Configuration of model compound **2A** of DmCry1 before (**2Aa**) and after (**2Ab**) proton transfer from Trp420 to FAD via Cys416.

doublet for **2Aa** and quartet for **2Ab** were assumed. Geometry changes were noted upon DFT optimization of the structure from the MD simulation's last trajectory. For example, for **2Aa**, the superposition of the isoalloxazine ring from MD- and DFT-optimized structures resulted in a small change with RMSD of 0.16 Å, and for the Trp residue the value was 0.08 Å. The N(W_n)−S(C416) and N5−S(C416) distances were modified, namely, 3.95 and 3.90 Å for the MD structure and 3.45 and 3.48 Å for the DFT-optimized structure, respectively (Table 1S in the SI). Although the relative orientation of the Trp residue changed from **2Aa** to **2Ab**, geometries of Trp and the isoalloxazine ring hardly varied, with a RMSD of 0.04 Å for both the isoalloxazine ring and Trp after superposition.

The gwCry1a structure was determined by homology modeling using the sequence of gwCry1a (GenBank accession no. AJ632120). X-ray crystal structures of the mouse mCry2 photolyase-homology region including FAD (pdb: 4I6G)[26] and of mCry1 without FAD (pdb: 4K0R),[27] were recently reported. Sequence alignment of gwCry1a and mCrys was performed with BLAST,[22] resulting in 88% identity with mCry1 and 81% identity with mCry2. Using the 3D structure of mCry2 (pdb: 4I6G) as a template, the 3D structure of gwCry1a was constructed with the SWISS-MODEL software[49] (shown in Figure 2S in the SI). On the basis of this structure, MD simulations were carried out with FAD in its oxidized state, where the protein was solvated in a box of dimensions 8.3 × 10.02 × 8.34 nm^3. The system was equilibrated for 100 ns at constant NVT (T = 300 K). Model compound **2B** (Figure 1) was based on the last structure of the MD trajectory, subsequently optimized with constrained boundary carbon atoms at the B3LYP/6-31G* level. Calculations for the AtCry1 model compound **2C** for comparison with gwCry1a were based on its X-ray structure (pdb: 1U3C, Figure 1)[23] and subsequent B3LYP/6-31G* DFT optimization. In Figure 3S in the SI, we show the geometry of isoalloxazine ring of $FAD^{\bullet-}$ in Dmcry1 ((a) last snapshot of 100 ns trajectory) and of FAD in its oxidized state in gwCry1a ((c) last snapshot of 100 ns trajectory). It is noted that the isoalloxazine ring is somewhat twisted in both cases, contrary to the planar geometry in the DmCry1 X-ray structure (Figure 3Sb in the SI) or the homology model (Figure 3Sd in the SI). Although a butterfly bent structure of anionic semiquinone FAD was demonstrated by QM/MM calculations of the *Bacillus cereus* NrdI enzyme,[50] the MD simulations depend on the force field used. However, the DFT-optimized geometries of **2Aa**, **2Ab**, and **2B** were also shown to deviate from planarity. (See Table 1S in the SI.)

II.3. pK_a. Calculations of pK_a for Asp396 in AtCry1 and Cys416 in DmCry1 were performed by evaluating the free-energy change upon so-called protein solvation as compared with aqueous solvation. The free-energy change associated with ionization of an acidic amino acid residue (AH) in a protein is $\Delta G^{p}(AH_p \rightarrow A_p^- + H_w^+) = \Delta G^{w}(AH_w \rightarrow A_w^- + H_w^+) + \Delta G_{sol}^{w\rightarrow p}(A^-) - \Delta G_{sol}^{w\rightarrow p}(AH)$, where p and w designate protein and water, respectively. The pK_a of a residue in a protein is given by $pK_{a,i}^{p} = pK_{a,i}^{w} - (\bar{q}_i/2.303RT)\Delta\Delta G_{sol}^{w\rightarrow p}(AH_i \rightarrow A_i^-)$, where $pK_{a,i}^{w}$ is 8.3 for the Cys group in solution and 3.9 for Asp, $\bar{q}_i$ is −1 for an acidic residue, and $\Delta\Delta G_{sol}^{w\rightarrow p}(AH_i \rightarrow A_i^-) = \Delta G_{sol}^{w\rightarrow p}(A_i^-) - \Delta G_{sol}^{w\rightarrow p}(AH_i)$. $\Delta G_{sol}^{w\rightarrow p}$(group) represents the free-energy difference of moving a group from water to its protein site. The PDLD/S (semimacroscopic protein dipoles Langevin dipoles)-linear response approximation[51] approach[52] was used to calculate the free-energy difference. In the PDLD approach, the system is divided into four regions: region I contains the active site, region II contains protein atoms that are close to region I, region III contains Langevin dipoles around region II that is further divided into inner and outer grids, and region IV is the bulk region around region III. The solvation of the active site is calculated by the electrostatic interaction between point charges in region I and point charges in region II and Langevin dipoles in region III and bulk water. Starting from an X-ray structure, the protein within 18 Å of the active site, commonly used,[53] was described with the ENZYMIX force field.[54] Parameters for FAD were assigned by matching to similar atom types in the force-field library. MD simulations using MOLARIS[54] at 300 K with a step size of 1 fs were performed for 100 ps. Configurations were recorded for each 1000 fs simulation and the pK_a calculated. The pK_a value was derived from an average of 100 results. The empirical PROPOKA3[55] method was used for comparison.

Because our objective was to compare the DmCry1 proximate residue's pK_a to that of Asp in the plant cryptochrome AtCry1,[29] we first validated pK_a predictions for Asp residues in comparison with available experimental values. This included Asp14 of the human pancreatic ribonuclease A (RNase A), whose crystal structure has been determined (pdb: 1KF2).[56] A pK_a of 2.0 was reported in this case.[57] In addition, Asp26 of the oxidized form of thioredoxin from *E. coli* (pdb: 2TRX)[58] with an experimental pK_a of 7.5[59] was considered. The calculated versus experimental pK_a results of 1.0 versus 2.0 for Asp14 of RNase A and 6.9 versus 7.5 for Asp26 of thioredoxin, respectively, demonstrate that the approach captures effects of the protein environment on the pK_a. The

DOI: 10.1021/jp508871h
J. Phys. Chem. B 2015, 119, 3883−3892

Table 3. Excitation Energies (eV) for Model Compounds 1B, 2Aa, and 2Ab, by CASSCF+XMCQDPT2 Calculations with FAD at the Semireduced State[a]

		D_0	LE^A_1	LE^A_2	LE^B_1	LE^B_2	LE^C_1	ET_I	ET_{II}
	Flavin	$\underline{0}\,\underline{0}$	$\underline{0}\,\underline{0}$	$\uparrow\underline{0}$	$\underline{0}\,\underline{0}$	$\underline{0}\,\underline{0}$	$\underline{0}\,\underline{0}$	$\underline{0}\,\underline{0}$	$\underline{0}\,\underline{0}$
		$\underline{0}\,\underline{0}$	$\uparrow\underline{0}$	$\underline{0}\,\underline{0}$	$\underline{0}\,\underline{0}$	$\underline{0}\,\underline{0}$	$0\downarrow$	$\underline{0}\,\underline{0}$	$0\downarrow$
Electron		$\uparrow\underline{0}$	$\underline{0}\,\underline{0}$	$\underline{0}\,\underline{0}$	$\uparrow\downarrow$	$\uparrow\downarrow$	$\uparrow\underline{0}$	$\uparrow\downarrow$	$\uparrow\underline{0}$
configuration		$\uparrow\downarrow$	$\uparrow\downarrow$	$\uparrow\downarrow$	$\uparrow\underline{0}$	$\uparrow\downarrow$	$\uparrow\underline{0}$	$\uparrow\downarrow$	$\uparrow\downarrow$
		$\uparrow\downarrow$	$\uparrow\downarrow$	$\uparrow\downarrow$	$\uparrow\downarrow$	$\uparrow\underline{0}$	$\uparrow\downarrow$	$\uparrow\downarrow$	$\uparrow\downarrow$
	Trp	$\uparrow\downarrow$	$\uparrow\downarrow$	$\uparrow\downarrow$	$\uparrow\downarrow$	$\uparrow\downarrow$	$\uparrow\downarrow$	$\uparrow\underline{0}$	$\uparrow\underline{0}$
Excitation energies	**1B**	0.0	0.98	2.38	2.46	2.85	3.51		
	2Aa	0.0			2.35		3.74	5.38	6.79
	2Ab	1.18[a]						1.73[a]	3.34[a]
	Experimental[64]		1.77~2.25		2.63	3.07	3.38		

[a]Electron configurations only include HOMO of Trp, LUMO+1, LUMO, SOMO (HOMO), HOMO-1, and HOMO-2 of flavin. Red, a hole due to an LE; green, occupied MO via excitation; purple, occupied MO by transferred electron. [b]Relative energy to ground-state of **2Aa**.

validated approach was used for calculating pK_a for the proximate residue in DmCry1 and AtCry1.

II.4. Electron Transfer within the Trp-Triad. The reaction free-energy and reorganization energy for modeling electron transfer, such as between Trp 420 (W_n) and Trp397 (W_m) (**1A** in Figure 1) as well as between Trp397 (W_m) and Trp 342 (W_f), were calculated by applying the linear response approximation, where the free-energy functions are parabolas of equal curvature, as found appropriate,[51,52] so that

$$\Delta G = 0.5(\langle V_B - V_A\rangle_A + \langle V_B - V_A\rangle_B) \quad (1)$$

$$\lambda = 0.5(\langle V_B - V_A\rangle_A - \langle V_B - V_A\rangle_B) \quad (2)$$

V_A (V_B) are the potential energies when the active site is in state A (B). In our case, A and B denote (W_n^+,W_m^0) and (W_n^0,W_m^+) for electron transfer from W_m to W_n and (W_m^+,W_f^0) and (W_m^0,W_f^+) for electron transfer from W_f to W_m; <> represents a sampling average from the MD simulations. The energy in eq 1 was obtained by the linear response approximation as follows. At each 100 ps interval, snapshots were used to calculate the energy difference between the two redox states, where, for instance, for redox state A, $\langle\rangle_A$ represents an average over trajectories from MD simulations of this redox state.

The potential energy of $V_{A(B)}$ does not include the internal energy of each redox partner (electron donor and acceptor) because the redox center is treated empirically, unlike in QM/MM MD simulations.[60] This internal contribution to the reorganization energy can be approximated as

$$\lambda^{\text{internal}} = 0.5\{(E^B - E^A)_A - (E^B - E^A)_B\} = 0.5\{E_A^B + E_B^A - E_A^A - E_B^B\} \quad (3)$$

where the superscript denotes the redox state and the subscript denotes the optimized geometry of the corresponding redox state. For the W_n–W_m pair, where A denotes the (W_n^+,W_m^0) redox state and B denotes the (W_n^0,W_m^+) redox state, $E_A^B = E[W_n^0]_{W_n^+} + E[W_m^+]_{W_m^0} = E[W^0]_{W^+} + E[W^+]_{W^0}$ and $E_A^A = E[W_n^+]_{W_n^+} + E[W_m^0]_{W_m^0} = E[W^+]_{W^+} + E[W^0]_{W^0}$. Similarly, we can get $E^A{}_B$ (equals to $E^B{}_A$) and $E^B{}_B$ (equals to $E^A{}_A$) so that $\lambda^{\text{internal}} = E_B^A - E_A^A$. A value of 0.33 eV was thus calculated at the B3LYP/6-31G* level using eq 3 and added to the values computed by eq 2. Such a small correction has been previously postulated.[61] The internal contribution to the free-energy difference is negligible because $\Delta G^{\text{internal}} = 0.5\{(E^B - E^A)_A + (E^B - E^A)_B\} = 0.5\{E_A^B - E_B^A - E_A^A + E_B^B\} = 0$.

MD simulations were carried out for 0.5 ns using MOLARIS with the polarizable ENZYMIX force field,[54] where the residues D, E, K, and R were ionized and explicit water was included. Taking into account polarization is important for calculation of the reorganization free-energy, λ, as was pointed out.[62] RESP charges for both neutral Trp and Trp^+ were derived using Ambertool 13[63] based on ROHF/6-31G* ESP calculations using the geometry optimized at the UB3LYP/6-31G* level. The simulated system was spherical, divided into four regions. Region I comprised W_nW_m or W_mW_f. Region II consisted of the unconstrained protein atoms and explicit water molecules up to 18 Å from the center of region I. In region III, a 2 Å shell of Langevin dipoles, embedding region II, was added. Region IV comprised a dielectric continuum that accounts for bulk effects. The standard surface-constrained solvent technique to account for the solvent and the reaction field for long-range treatment were applied.

III. RESULTS AND DISCUSSION

III.1. Radical-Pair Formation in Semireduced DmCry1. First, the electronic excitations of anionic semiquinone $FAD^{\bullet-}$ were investigated using the optimized model compound **1B**, as described in Section II.2. As we previuosly stated, LUMO+1, LUMO, HOMO (SOMO), HOMO-1, and HOMO-2 were included in the CASSCF/6-311G* calculation, resulting in 75 doublet states, which were all included in the state-averaged CASSCF calculation. The first five excitation states were identified as being one of three excitation types: electron excited from a SOMO to an unoccupied MO LE^A (LE: local excitation on isoalloxazine ring), from a doubly occupied MO to a SOMO (LE^B), and from a doubly occupied MO to an unoccupied MO (LE^C). The CASSCF/XMCQDPT2 excitation energies of **1B** are listed in Table 3, where the radical is on the flavin. Transitions LE^A_1 (0.98 eV) and LE^A_2 (2.38 eV) were assigned to the experimentally observed weak absorption in the range of 1.77 to 2.25 eV, and LE^B_1 (2.46 eV), LE^B_2 (2.85 eV),

DOI: 10.1021/jp508871h
J. Phys. Chem. B 2015, 119, 3883−3892

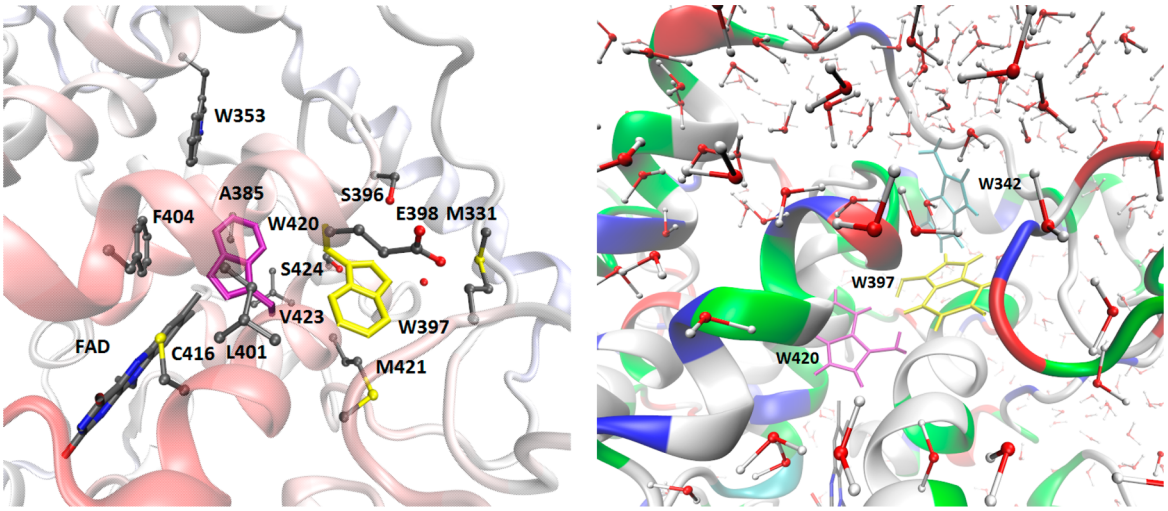

Figure 3. (a) Local environment of W420 and W397, showing a hydrophobic cage for W420 and hydrophilic environment around W397. (b) Trp-triad within protein. W342 is shown to be closer to the surface than W397 and W420.

and LE^{C}_{1} (3.51 eV) were assigned to three strong absorption peaks of 2.63, 3.07, and 3.38 eV, respectively.[64]

Excitation energies LE^{B}_{1} (2.35 eV) and of LE^{C}_{1} (3.74 eV) for **2Aa** are close to the results using model **1B** and lower than those of ET_{I} (ET: electron transfer from W_n to isoalloxazine ring) and ET_{II}. (See Table 3.) When considering proton transfer in conjunction with electron transfer using model compound **2Ab**, in which W420 was deprotonated and flavin was protonated at N5, the ground state of **2Ab** is higher in energy than that of **2Aa** by 1.18 eV (Table 3; interestingly, a UMP2/6-31+G* calculation using the same geometry resulted in **2Ab** having an energy 1.19 eV higher than for **2Aa**). In both cases, the flavin moiety is a radical and the Trp residue is in a closed-shell configuration. The energy of the ET_{I} state of **2Ab** was found to be lower than LE^{B}_{1} of **2Aa** by 0.6 eV, and the energy of ET_{II} of **2Ab** was found to be lower than LE^{C}_{1} of **2Aa** by 0.4 eV, implying that LE^{B}_{1} photoexcitation can possibly induce ET_{I} and LE^{C}_{1} ET_{II}, respectively. The flavin moiety of ET_{II} is a radical with two SOMOs, which could form a radical pair with a Trp radical.[65] Note that for both ET_{I} and ET_{II} states of model compound **2Ab**, the FAD is in the fully reduced form ($FADH^{-}$), which is not uncommon, because photolyase also uses $FADH^{-}$ to repair UV-damaged DNA, where electron transfer from $FADH^{-}$ to mutagenic photolesions from adjacent pyrimidine bases in DNA are formed due to UV exposure.[66,67]

III.2. pK_a of Proximate Residue to FAD and Trp-Triad. We note here that quantification of the pK_a of the proximate residue in the active site within the protein environment is also important because it indicates residues' propensity toward proton transfer. Our validated pK_a results from the free-energy change upon incorporation of the residue in the cryptochrome (see Section II.3 for computational details) resulted in values of 7.6 for Asp396 in AtCry1 and 9.7 for Cys416 in DmCry1, respectively. The corresponding values using the empirical method PROPOKA3 were 9.7 and 12.9 for Asp396 in AtCry1 and Cys416 in DmCry1, respectively. A smaller difference in the pK_a between AtCry1 and DmCry1 is thus noted, as compared with values of the amino acids in aqueous solution (pK_a of 3.9 for Asp and 8.3 for Cys),[64] indicating that the difference in proton transfer affinity of Cys416 in DmCry1 compared with Asp396 in AtCry1 is not as large, as was anticipated from solution values, and Asp396 in AtCry1 was reported to act as a proton donor to the semireduced flavin $FAD^{\bullet-}$ in AtCry1,[68,69] so it might be possible for Cys416 to donate a proton.

To ensure that feasibility of proton transfer from C416 to N5 of the $FAD^{\bullet-}$ isoalloxazine ring, we considered model compounds **3A1** and **3A2** (shown in Figure 4S in the SI), which have extended model compound **2A** with the additional proximate residues R361, D410, and S267, optimized at the UB3LYP/6-31+G*level. The ground-state energy (UB3LYP/6-31+G*) for **3A2**, where the proton has been transferred from C416 to N5 of FAD, is 0.20 eV higher in energy than for **3A1**, while when these three residues were not included the number became 0.24 eV. It is reasonable to assume that ptotonation of N5 of $FAD^{\bullet-}$ is possible.

III.3. Electron Transfer within Trp-Triad in DmCry1. The feasibility of a radical-pair mechanism is dependent on fast electron transfer within the Trp-triad, or so-called "nanowire", to enable the separation of the radical-pair partners, reducing dipolar and exchange interactions. Calculations of the rate of electron transfer (k_{ET}) were based on Marcus's theory,[70] given by $\log(k_{ET}) = 15 - 0.434\beta R - 3.1[(\Delta G + \lambda)^2/\lambda]$, where ΔG and λ are the Gibbs free-energy and reorganization energy (eV), respectively. These values were calculated by the linear response approximation from MD simulations, as described Section II.4. A β value of 1.4 $Å^{-1}$ is often assumed,[71] an intermediate between doped semiconductors and vacuum.[72] R is the edge-to-edge distance between the two Trp ring heavy atoms (Figure 1S in the SI).

MD simulations for evaluation of V_A and V_B (eqs 1 and 2 in Section II.4) were carried out for both electron transfer from W_m to W_n and from W_f to W_m for a duration of 0.5 ns, and trajectories of the last 0.4 ns were analyzed assuming the linear response approximation, as shown in Figure 5S in the SI. ΔG for electron transfer from W397 (W_m) to W420 (W_n) was calculated as −7.0 kcal. Analysis indicated that compared with the (W_n^{+},W_m) redox state, (W_n,W_m^{+}) is stabilized by the protein environment by −2.8 kcal/mol and by water solvation by −4.2 kcal/mol. These results are consistent with the

DOI: 10.1021/jp508871h
J. Phys. Chem. B 2015, 119, 3883−3892

observation that W420 (W_n) is buried in a more hydrophobic pocket, while W397(W_m) is in a hydrophilic cage (shown in Figure 3a) and closer to the surface, and a positive charge at W420 would be less solvated by the protein and water than a positive charge at W397. For electron transfer from W342 (W_f) to W397 (W_m), a reaction free-energy value of −5.3 kcal was calculated, where the protein environment contributed 11.1 kcal/mol and water solvation contributed −16.4 kcal/mol, consistent with the fact that W342 is closer to the protein surface and more exposed and solvated by water. (See Figure 3b.) It was indeed previously noted that residues nearby W_m can make an important contribution in stabilizing ionized W_m in Atcry1.[8]

Using the above equation,[70] with an edge-to-edge distance of 4.7 Å (Figure 1S in the SI), we estimated k_{ET} from W397 to W420 to be 330, 190, and 4 ns^{-1} for β values of 1.4, 1.5, and 2.3 $Å^{-1}$, respectively. The calculated reorganization energy, λ, was 0.68 eV for electron transfer from W397 to W420 and 0.78 eV for electron transfer from W342 (W_f) to W397 (W_m). When an edge-to-edge distance of 4.55 Å from the MD simulation averaged results was used, the corresponding k_{ET} from W397 to W420 was 374, 237, and 6 ns^{-1} for β values of 1.4, 1.5, and 2.3 $Å^{-1}$, showing minor changes. Dependent on accurate estimation of β, results are qualitatively consistent with an experimental k_{ET} from W_m to W_n^+ in the insect cryptochrome from *Antheraea pernyi* (ApCry1) of 16 ns^{-1}[73] (with 55% sequence identity with DmCry1) and similarly from W_m to W_n^+ (14 ns^{-1}) in *E. coli* DNA photolyase.[74] We point out that the electron transfer rate from W_m to W_n was suggested to range from 0.1 to 1 ns^{-1} in AtCry1[8] (with 29% sequence identity with DmCry1). The k_{ET} from W342 to W397 was calculated to be 353, 244, and 13 ns^{-1} for β values of 1.4, 1.5, and 2.3 $Å^{-1}$, assuming an edge-to-edge distance of 3.7 Å (Figure 1S in the SI), while when an average from the MD results was used (edge-to-edge distance of 3.87 Å), corresponding values were 278, 189, and 8 ns^{-1} for β values of 1.4, 1.5, and 2.3 $Å^{-1}$, respectively. Although we do not have direct comparison to experiment, fast electron transfer from W_f to W_m (7 ns^{-1}) in *E. coli* DNA photolyase was reported, where W_f was exposed to the solvent, similar to DmCry1.[74]

III.4. Radical-Pair Formation in gwCry1. To further explore cryptochromes from species that demonstrate magnetoreception, we analyzed photoexcitation followed by electron transfer from W_n to oxidized FAD in gwCry1a compared with results for AtCry1.[29] Model compound **2B** of gwCry1a (Figure 1) was used, with the initial structure derived as described in Section II.2 Optimization of the S_0 ground-state and T_1 triplet excited-state geometries of **2B** were performed using UB3LYP/6-31G* and for the singlet excited-state S_1 using TDDFT with B3LYP/6-31G*. For consistency, the B3LYP functional was chosen for the TDDFT geometry optimization to examine the trend, although it is known to be problematic for charge-transfer excitations.[41,75] Note that the optimized structure of S_1 by TDDFT/B3LYP can be presumed to be a minimum because it is consistent with a similar computation for a BLUF (blue light using FAD) protein model compound.[75] Structural alignment of the S_0 and S_1 minima for the isoalloxazine ring and Trp residue of **2B** resulted in a RMSD value of 0.04 Å, showing minimal deviation. However, the H(W_n)−O(N393), O4(flavin)−H(N393), and H3′(ribityl)−N1 distances are shorter in the S_1 versus S_0 geometry, changing from 1.92, 2.00, and 1.92 Å to 1.51, 1.73, and 1.84 Å, respectively (Table 1S in the SI), stabilizing a W_n^+ flavin$^-$ structure because of strong hydrogen-bond interactions. For the T1 minimum, the H(W_n)−O(N393), O4(flavin)−H(N393), and H3′(ribityl)−N1 distances are 1.72, 1.87, and 1.92 Å, respectively, larger than the corresponding values for the S_1−ET geometry by 0.21, 0.14, and 0.08 Å, respectively.

Excitation energies were calculated using CASSCF/6-31G* (four electrons, three orbitals, and three electronic states)-XMCQDPT2, summarized in Table 2S in the SI. Frontier natural orbitals (NOs) of S_1 from the state-averaged CASSCF calculations for model compound **2B** of gwCry1a using S_0- (a) and S_1- (b) optimized geometries are shown in Figure 4. The

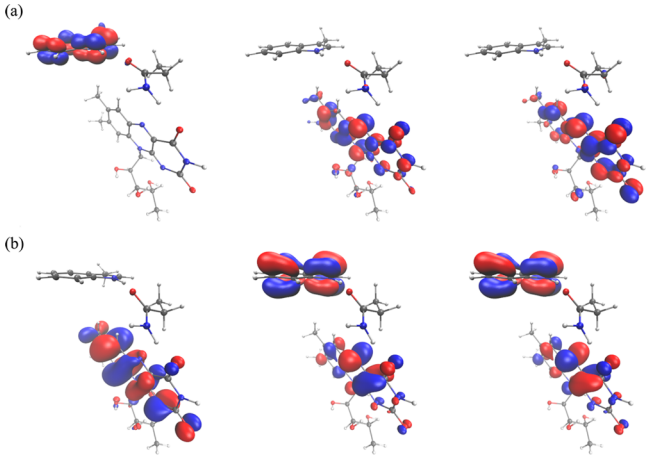

Figure 4. Frontier NOs of S_1 from state-averaged CASSCF calculations for model compound **2B** of gwCry1a using (a) DFT S_0- and (b) TDDFT S_1-optimized geometries, as described in the text.

occupation numbers for NOs 149, 150, and 151 (left to right in Figure 4) are 2.000, 1.289, and 0.711 for (a) and 2.000, 1.002, and 0.998 for (b). When the TDDFT-optimized S_1 geometry was used, the doubly occupied NO #149 was localized on the isoalloxazine ring and S_1 was due to electron transfer from W397 to flavin (S^{ET}) (Figure 4b), but when using the S_0 DFT-optimized geometry, it was localized on W397 (Figure 4a) and S_1 was attributed to a local electronic excitation within flavin ring (S^{LE}). Using the S_0 geometry, the $S_0 \rightarrow S^{LE}$ excitation energy was calculated as 2.71 eV, which is close to the experimental value of 2.8 eV for gwCry1a,[20] but S^{ET} was higher in energy than the S^{LE} state by 0.31 eV. However, in using an optimized geometry for S_1 and for T_1, the S^{ET} energies were lower than those of the S^{LE} state by 0.80 and 0.03 eV, respectively. Electron transfer from Trp to FAD* is thus energetically favorable with an optimized excited-state geometry. Similarly, for the model compound of AtCry1 (**2C** in Figure 1), using the S_0 geometry, the $S_0 \rightarrow S^{LE}$ excitation energy was 2.64 eV, with S^{ET} 0.29 eV higher in energy than S^{LE}, while when using the T_1 geometry, S^{ET} was 0.21 eV lower in energy than S^{LE}. A similar trend was previously reported for AtCry1 in the work by Solov'yov et al.,[29] although a different model compound and geometry optimization method were used. In that case, using the optimized geometry of S_0, S^{ET} was 0.83 eV higher than S^{LE}, while when using the optimized geometry of S^{ET}, S^{ET} was 0.20 eV lower than the S^{LE} state.[29]

IV. CONCLUSIONS

Investigation of the photoexcitation and electron transfer in the FAD—Trp-triad active site of DmCry1 provided support, in part, of a radical-pair mechanism using a combination of

DOI: 10.1021/jp508871h
J. Phys. Chem. B 2015, 119, 3883−3892

theoretical methods, ranging from high-level ab initio to free-energy MD simulations with a polarizable force field. Results were validated in comparison with experimental data as available. Excitation energies followed by electron transfer, investigated at the CASSCF-XMCQDPT2/6-311G(d) level for model compounds of the active site, assuming proton transfer in conjunction with electron transfer from W420 to FAD, found the mechanism to be energetically favorable. The predicted pK_a of Cys416 in DmCry1, as compared with the respective value for Asp396 in AtCry1, also potentially supports such a mechanism. Electron transfer within the Trp-triad in DmCry1, studied by MD simulations assuming the linear response approximation for evaluation of the reaction free energy and reorganization energy, demonstrated facile electron transfer due to the local protein environment and solvent exposure. This can be attributed to the observation that W_n is embedded in a hydrophobic cage, W_m is surrounded by a hydrophilic environment, and W_f is closer to the protein surface and thus more exposed to the solvent. The calculated electron-transfer rates are qualitatively consistent with experimental data for related proteins. Finally, light-induced electron transfer from proximate Trp to FAD was investigated for gwCry1a for a model compound derived from a protein structure determined by homology modeling and refined by MD simulation, followed by DFT optimization, demonstrating that for relaxed excited-state geometries, the mechanism could be feasible in the first stage. Overall, our results provide an understanding of the radical-pair mechanism for cryptochromes from species other than from the plant *Arabidopsis thaliana*, investigated in the pioneering work of Solov'yov et al.,[8,29] specifically from the insect *Drosophila melanogaster* and the bird *Sylvia borin*.

■ ASSOCIATED CONTENT

Supporting Information

Geometrical parameters of model compounds. CASSCF-XMCQDPT2 total energies for model compound **2B**. Distances used in derivation of electron transfer rate in DmCry1. Homology model for gwCry1a. Geometries of isoalloxazine ring of $FAD^{\bullet-}$ in DmCry1 and FAD_{ox} in gwCry1a as derived from the MD simulation and crystal structure. Larger model compounds for proton transfer from C416 to FAD. Averaging procedure for linear response approximation calculation. This material is available free of charge via the Internet at http://pubs.acs.org.

■ AUTHOR INFORMATION

Corresponding Author

*E-mail: ruth.pachter@us.af.mil. Tel: (937) 255-9689.

Notes

The authors declare no competing financial interest.

■ ACKNOWLEDGMENTS

We gratefully acknowledge support from the Air Force Office of Scientific Research and computational resources and helpful assistance provided by the AFRL DSRC.

■ REFERENCES

(1) Johnsen, S.; Lohmann, K. J. The Physics and Neurobiology of Magnetoreception. *Nat. Rev. Neurosci.* **2005**, *6*, 703−712.
(2) Mouritsen, H.; Hore, P. The Magnetic Retina: Light-dependent and Trigeminal Magnetoreception in Migratory Birds. *Curr. Opin. Neurobiol.* **2012**, *22*, 343−352.
(3) Wiltschko, W.; Wiltschko, R. Magnetic Compass of European Robins. *Science* **1972**, *176*, 62−64.
(4) Chaves, I.; Pokorny, R.; Byrdin, M.; Hoang, N.; Ritz, T.; Brettel, K.; Essen, L.-O.; van der Horst, G. T. J.; Batschauer, A.; Ahmad, M. The Cryptochromes: Blue Light Photoreceptors in Plants and Animals. *Annu. Rev. Plant Biol.* **2011**, *62*, 335−364.
(5) Ritz, T.; Adem, S.; Schulten, K. A Model for Photoreceptor-based Magnetoreception in Birds. *Biophys. J.* **2000**, *78*, 707−718.
(6) Dodson, C. A.; Hore, P. J.; Wallace, M. I. A Radical Sense of Direction: Signalling and Mechanism in Cryptochrome Magneto-reception. *Trends Biochem. Sci.* **2013**, *38*, 435−446.
(7) Tierschi, M.; Briegel, H. J. Decoherence in the Chemical Compass: The Role of Decoherence for Avian Magnetoreception. *Philos. Trans. R. Soc., A* **2012**, *370*, 4517−4540.
(8) Solov'yov, I. A.; Domratcheva, T.; Schulten, K. Separation of Photo-induced Radical Pair in Cryptochrome to a Functionally Critical Distance. *Sci. Rep.* **2014**, *4*, 1−8.
(9) Efimova, O. E.; Hore, P. J. The Role of Exchange and Dipolar Interactions in the Radical Pair Model of the Avian Magnetic Compass. *Biophys. J.* **2008**, *94*, 1565−1574.
(10) Biskup, T. Time-resolved EPR of Radical Pair Intermediates in Cryptochromes. *Mol. Phys.* **2013**, *111*, 3698−3703.
(11) Wiltschko, R.; Dehe, L.; Gehring, D.; Thalau, P.; Wiltschko, W. Interactions Between the Visual and the Magnetoreception System: Different Effects of Bichromatic Light Regimes on the Directional Behavior of Migratory Birds. *J. Physiol. Paris* **2013**, *107*, 137−146.
(12) Ritz, T.; Wiltschko, R.; Hore, P. J.; Rodgers, C. T.; Stapput, K.; Thalau, P.; Timmel, C. R.; Wiltschko, W. Magnetic Compass of Birds Is Based on a Molecule with Optimal Directional Sensitivity. *Biophys. J.* **2009**, *96*, 3451−3457.
(13) Maeda, K.; Henbest, K. B.; Cintolesi, F.; Kuprov, I.; Rodgers, C. T.; Liddell, P. A.; Gust, D.; Timmel, C. R.; Hore, P. J. Chemical Compass Model of Avian Magnetoreception. *Nature* **2008**, *453*, 387−390.
(14) Maeda, K.; Robinson, A. J.; Henbest, K. B.; Hogben, H. J.; Biskup, T.; Ahmad, M.; Schleicher, E.; Weber, S.; Timmel, C. R.; Hore, P. J. Magnetically Sensitive Light-induced Reactions in Cryptochrome are Consistent with its Proposed Role as a Magneto-receptor. *Proc. Natl. Acad. Sci. U. S. A.* **2012**, *109*, 4774−4779.
(15) Solov'yov, I. A.; Schulten, K. Reaction Kinetics and Mechanism of Magnetic Field Effects in Cryptochrome. *J. Phys. Chem. B* **2011**, *116*, 1089−1099.
(16) Hill, E.; Ritz, T. Can disordered Radical Pair Systems Provide a Basis for a Magnetic Compass in Animals? *J. R. Soc. Interface* **2010**, *7*, S265−S271.
(17) Cai, J.; Guerreschi, G. G.; Briegel, H. J. Quantum Control and Entanglement in a Chemical Compass. *Phys. Rev. Lett.* **2010**, *104* (220502), 1−4.
(18) Hogben, H. J.; Biskup, T.; Hore, P. J. Entanglement and Sources of Magnetic Anisotropy in Radical Pair-based Avian Magnetoreceptors. *Phys. Rev. Lett.* **2012**, *109* (22050), 1−5.
(19) Gegear, R. J.; Casselman, A.; Waddell, S.; Reppert, S. M. Cryptochrome Mediates Light-dependent Magnetosensitivity in Drosophila. *Nature* **2008**, *454*, 1014−1018.
(20) Liedvogel, M.; Maeda, K.; Henbest, K.; Schleicher, E.; Simon, T.; Timmel, C. R.; Hore, P. J.; Mouritsen, H. Chemical Magneto-reception: Bird Cryptochrome 1a Is Excited by Blue Light and Forms Long-Lived Radical-Pairs. *PLoS One* **2007**, *2*, e1106/1−7.
(21) Zhang, Y.; Skolnick, J. TM-align: A Protein Structure Alignment Algorithm Based on the TM-Score. *Nucleic Acids Res.* **2005**, *33*, 2302−2309.
(22) Altschul, S. F.; Madden, T. L.; Schäffer, A. A.; Zhang, J.; Zhang, Z.; Miller, W.; Lipman, D. J. Gapped BLAST and PSI-BLAST: A New Generation of Protein Database Search Programs. *Nucleic Acids Res.* **1997**, *25*, 3389−3402.
(23) Brautigam, C. A.; Smith, B. S.; Ma, Z.; Palnitkar, M.; Tomchick, D. R.; Machius, M.; Deisenhofer, J. Structure of the Photolyase-like Domain of Cryptochrome 1 from Arabidopsis Thaliana. *Proc. Natl. Acad. Sci. U. S. A.* **2004**, *101*, 12142−12147.

DOI: 10.1021/jp508871h
J. Phys. Chem. B 2015, 119, 3883−3892

(24) Zoltowski, B. D.; Vaidya, A. T.; Top, D.; Widom, J.; Young, M. W.; Crane, B. R. Structure of Full-length Drosophila Cryptochrome. *Nature* **2011**, *480*, 396−399.
(25) Levy, C.; Zoltowski, B. D.; Jones, A. R.; Vaidya, A. T.; Top, D.; Widom, J.; Young, M. W.; Scrutton, N. S.; Crane, B. R.; Leys, D. Updated Structure of Drosophila Cryptochrome. *Nature* **2013**, *495*, E3−E4.
(26) Xing, W.; Busino, L.; Hinds, T. R.; Marionni, S. T.; Saifee, N. H.; Bush, M. F.; Pagano, M.; Zheng, N. SCFFBXL3 Ubiquitin Ligase Targets Cryptochromes at their Cofactor Pocket. *Nature* **2013**, *496*, 64−68.
(27) Czarna, A.; Berndt, A.; Singh, Hari R.; Grudziecki, A.; Ladurner, Andreas G.; Timinszky, G.; Kramer, A.; Wolf, E. Structures of Drosophila Cryptochrome and Mouse Cryptochrome1 Provide Insight into Circadian Function. *Cell* **2013**, *153*, 1394−1405.
(28) Page, C. C.; Moser, C. C.; Chen, X.; Dutton, P. L. Natural Engineering Principles of Electron Tunneling in Biological Oxidation-reduction. *Nature* **1999**, *402*, 47−52.
(29) Solov'yov, I. A.; Domratcheva, T.; Moughal Shahi, A. R.; Schulten, K. Decrypting Cryptochrome: Revealing the Molecular Identity of the Photoactivation Reaction. *J. Am. Chem. Soc.* **2012**, *134*, 18046−18052.
(30) Ozturk, N.; Selby, C. P.; Annayev, Y.; Zhong, D.; Sancar, A. Reaction Mechanism of Drosophila Cryptochrome. *Proc. Natl. Acad. Sci. USA* **2011**, *108*, 516−521.
(31) Gegear, R. J.; Foley, L. E.; Casselman, A.; Reppert, S. M. Animal Cryptochromes Mediate Magnetoreception by an Unconventional Photochemical Mechanism. *Nature* **2010**, *463*, 804−807.
(32) Schmidt, M. W.; Gordon, M. S. The Construction and Interpretation of MCSCF Wavefunctions. *Annu. Rev. Phys. Chem.* **1998**, *49*, 233−266.
(33) Granovsky, A. A. Extended Multi-configuration Quasi-degenerate Perturbation Theory: The New Approach to Multi-state Multi-reference Perturbation Theory. *J. Chem. Phys.* **2011**, *134* (214113), 1−14.
(34) Nakano, H. Quasidegenerate Perturbation Theory with Multiconfigurational Self-Consistent-Field Reference Functions. *T J. Chem. Phys.* **1993**, *99*, 7983−7992.
(35) Granovsky, A. A. *Firefly*, version 8.0.0. http://classic.chem.msu.su/gran/gamess/index.html.
(36) Schmidt, M. W.; et al. General Atomic and Molecular Electronic Structure System. *J. Comput. Chem.* **1993**, *14*, 1347−1363.
(37) Udvarhelyi, A.; Domratcheva, T. Photoreaction in BLUF Receptors: Proton-coupled Electron Transfer in the Flavin-Gln-Tyr System. *Photochem. Photobiol.* **2011**, *87*, 554−563.
(38) Bode, B. M.; Gordon, M. S. Macmolplt: A Graphical User Interface for GAMESS. *J. Mol. Graph. Model.* **1998**, *16*, 133−138.
(39) Frisch, M. J.; et al. *Gaussian 09*;Gaussian, Inc.: Wallingford, CT, 2009.
(40) Stratmann, R. E.; Scuseria, G. E.; Frisch, M. J. An Efficient Implementation of Time-Dependent Density-Functional Theory for the Calculation of Excitation Energies of Large Molecules. *J. Chem. Phys.* **1998**, *109*, 8218−8224.
(41) Nguyen, K. A.; Day, P. N.; Pachter, R. The Performance and Relationship Among Range-Separated Schemes for Density Functional Theory. *J. Chem. Phys.* **2011**, *135*, 074101−074110.
(42) Kao, Y.-T.; Saxena, C.; He, T.-F.; Guo, L.; Wang, L.; Sancar, A.; Zhong, D. Ultrafast Dynamics of Flavins in Five Redox States. *J. Am. Chem. Soc.* **2008**, *130*, 13132−13139.
(43) Humphrey, W.; Dalke, A.; Schulten, K. VMD: Visual Molecular Dynamics. *J. Mol. Graph. Model.* **1996**, *14*, 33−38.
(44) Singh, U. C.; Kollman, P. A. An Approach to Computing Electrostatic Charges for Molecules. *J. Comput. Chem.* **1984**, *5*, 129−145.
(45) Hess, B.; Kutzner, C.; van der Spoel, D.; Lindahl, E. GROMACS 4: Algorithms for Highly Efficient, Load-Balanced, and Scalable Molecular Simulation. *J. Chem. Theory Comput.* **2008**, *4*, 435−447.
(46) Hornak, V.; Abel, R.; Okur, A.; Strockbine, B.; Roitberg, A.; Simmerling, C. Comparison of Multiple Amber Force Fields and Development of Improved Protein Backbone Parameters. *Proteins* **2006**, *65*, 712−725.
(47) Wang, J.; Wolf, R. M.; Caldwell, J. W.; Kollman, P. A.; Case, D. A. Development and Testing of a General Amber Force Field. *J. Comput. Chem.* **2004**, *25*, 1157−1174.
(48) Hess, B.; Bekker, H.; Berendsen, H. J. C.; Fraaije, J. G. E. M. LINCS: A Linear Constraint Solver for Molecular Simulations. *J. Comput. Chem.* **1997**, *18*, 1463−1472.
(49) Arnold, K.; Bordoli, L.; Kopp, J.; Schwede, T. The SWISS-MODEL Workspace: A Web-based Environment for Protein Structure Homology Modelling. *Bioinformatics* **2006**, *22*, 195−201.
(50) Røhr, Å. K.; Hersleth, H.-P.; Andersson, K. K. Tracking Flavin Conformations in Protein Crystal Structures with Raman Spectroscopy and QM/MM Calculations. *Angew. Chem., Int. Ed.* **2010**, *122*, 2374−2377.
(51) King, G. Warshel. Investigation of the Free-Energy Functions for Electron-Transfer Reactions. *J. Chem. Phys.* **1990**, *93*, 8682−8692.
(52) Sham, Y. Y.; Chu, Z. T.; Tao, H.; Warshel, A. Examining Methods for Calculations of Binding Free Energies: LRA, LIE, PDLD-LRA, and PDLD/S-LRA Calculations of Ligands Binding to an HIV Protease. *Proteins* **2000**, *39*, 393−407.
(53) Olsson, M. H. M.; Hong, G.; Warshel, A. Frozen Density Functional Free Energy Simulations of Redox Proteins: Computational Studies of the Reduction Potential of Plastocyanin and Rusticyanin. *J. Am. Chem. Soc.* **2003**, *125*, 5025−5039.
(54) Lee, F. S.; Chu, Z. T.; Warshel, A. Microscopic and Semimicroscopic Calculations of Electrostatic Energies in Proteins by the POLARIS and ENZYMIX Programs. *J. Comput. Chem.* **1993**, *14*, 161−185.
(55) Olsson, M. H. M.; Søndergaard, C. R.; Rostkowski, M.; Jensen, J. H. PROPKA3: Consistent Treatment of Internal and Surface Residues in Empirical pKa Predictions. *J. Chem. Theory Comput.* **2011**, *7*, 525−537.
(56) Berisio, R.; Sica, F.; Lamzin, V. S.; Wilson, K. S.; Zagari, A.; Mazzarella, L. Atomic Resolution Structures of Ribonuclease A at Six pH Values. *Acta Crystallogr., D* **2002**, *58*, 441−450.
(57) Baker, W. R.; Kintanar, A. Characterization of the pH Titration Shifts of Ribonuclease A by One- and Two-Dimensional Nuclear Magnetic Resonance Spectroscopy. *Arch. Biochem. Biophys.* **1996**, *327*, 189−199.
(58) Katti, S. K.; LeMaster, D. M.; Eklund, H. Crystal Structure of Thioredoxin from Escherichia coli at 1.68 Å Resolution. *J. Mol. Biol.* **1990**, *212*, 167−184.
(59) Langsetmo, K.; Fuchs, J. A.; Woodward, C. The Conserved, Buried Aspartic Acid in Oxidized Escherichia coli Thioredoxin has a pKa of 7.5. Its Titration Produces a Related Shift in Global Stability. *Biochemistry* **1991**, *30*, 7603−7609.
(60) Hong, G.; Ivnitski, D. M.; Johnson, G. R.; Atanassov, P.; Pachter, R. Design Parameters for Tuning the Type 1 Cu Multicopper Oxidase Redox Potential: Insight from a Combination of First Principles and Empirical Molecular Dynamics Simulations. *J. Am. Chem. Soc.* **2011**, *133*, 4802−4809.
(61) Woiczikowski, P. B.; Steinbrecher, T.; Kubar, T.; Elstner, M. Nonadiabatic QM/MM Simulations of Fast Charge Transfer in Escherichia coli DNA Photolyase. *J. Phys. Chem. B* **2011**, *115*, 9846−9863.
(62) Blumberger, J. Free Energies for Biological Electron Transfer from QM/MM Calculation: Method, Application and Critical Assessment. *Phys. Chem. Chem. Phys.* **2008**, *10*, 5651−5667.
(63) Case, D. A.; et al. *AMBER 13*; University of California: San Francisco, 2012.
(64) Berndt, A.; Kottke, T.; Breitkreuz, H.; Dvorsky, R.; Hennig, S.; Alexander, M.; Wolf, E. A Novel Photoreaction Mechanism for the Circadian Blue Light Photoreceptor Drosophila Cryptochrome. *J. Biol. Chem.* **2007**, *282*, 13011−13021.
(65) Steiner, U. E.; Ulrich, T. Magnetic Field Effects in Chemical Kinetics and Related Phenomena. *Chem. Rev.* **1989**, *89*, 51−147.

DOI: 10.1021/jp508871h
J. Phys. Chem. B 2015, 119, 3883−3892

(66) Sadeghian, K.; Bocola, M.; Merz, T.; Schütz, M. Theoretical Study on the Repair Mechanism of the (6−4) Photolesion by the (6−4) Photolyase. *J. Am. Chem. Soc.* **2010**, *132*, 16285−16295.
(67) Kao, Y.-T.; Saxena, C.; Wang, L.; Sancar, A.; Zhong, D. Direct Observation of Thymine Dimer Repair in DNA by Photolyase. *Proc. Natl. Acad. Sci. U. S. A.* **2005**, *102*, 16128−16132.
(68) Langenbacher, T.; Immeln, D.; Dick, B.; Kottke, T. Microsecond Light-Induced Proton Transfer to Flavin in the Blue Light Sensor Plant Cryptochrome. *J. Am. Chem. Soc.* **2009**, *131*, 14274−14280.
(69) Kottke, T.; Batschauer, A.; Ahmad, M.; Heberle, J. Blue-Light-Induced Changes in Arabidopsis Cryptochrome 1 Probed by FTIR Difference Spectroscopy. *Biochemistry* **2006**, *45*, 2472−2479.
(70) Marcus, R. A.; Sutin, N. Electron Transfers in Chemistry and Biology. *Biochim. Biophys. Acta* **1985**, *811*, 265−322.
(71) Moser, C. C.; Keske, J. M.; Warncke, K.; Farid, R. S.; Dutton, P. L. Nature of Biological Electron Transfer. *Nature* **1992**, *355*, 796−802.
(72) Edwards, P. P.; Gray, H. B.; Lodge, M. T. J.; Williams, R. J. P. Electron Transfer and Electronic Conduction Through an Intervening Medium. *Angew. Chem., Int. Ed.* **2008**, *47*, 6758−6765.
(73) Kao, Y.-T.; Tan, C.; Song, S.-H.; Oztuerk, N.; Li, J.; Wang, L.; Sancar, A.; Zhong, D. Ultrafast Dynamics and Anionic Active States of the Flavin Cofactor in Cryptochrome and Photolyase. *J. Am. Chem. Soc.* **2008**, *130*, 7695−7701.
(74) Liu, Z.; Tan, C.; Guo, X.; Li, J.; Wang, L.; Sancar, A.; Zhong, D. Determining Complete Electron Flow in the Cofactor Photoreduction of Oxidized Photolyase. *Proc. Natl. Acad. Sci. U. S. A.* **2013**, *110*, 12966−12971.
(75) Sadeghian, K.; Bocola, M.; Schutz, M. A Conclusive Mechanism of the Photoinduced Reaction Cascade in Blue Light Using Flavin Photoreceptors. *J. Am. Chem. Soc.* **2008**, *130*, 12501−12513.

DOI: 10.1021/jp508871h
J. Phys. Chem. B 2015, 119, 3883−3892